J Sci Comput
DOI 10.1007/s10915-015-0085-5

A Simplified Formulation of the Flux Reconstruction Method

J. Romero[1] · **K. Asthana**[1] · **A. Jameson**[1]

Received: 17 December 2014 / Revised: 13 June 2015 / Accepted: 18 August 2015
© Springer Science+Business Media New York 2015

Abstract The flux reconstruction (FR) methodology has proved to be an attractive approach to obtaining high-order solutions to hyperbolic partial differential equations. However, the utilization of somewhat arbitrarily defined correction polynomials in the application of these schemes, while adding some flexibility, detracts from their ease of implementation and computational efficiency. This paper describes a simplified formuation of the flux reconstruction method that replaces the application of correction polynomials with a single Lagrange interpolation operation. A proof of the algebraic equivalence of this scheme to the FR formulation of the nodal discontinuous Galerkin (DG) method provided that the interior solution points are placed at the zeros of a corresponding Legendre polynomial is presented. Next, a proof of linear stability for this formulation is given. Subsequently, von Neumann analysis is carried out on the new formulation to identify a range of linearly stable schemes achieved by variations of the interior solution point locations. This analysis leads to the discovery of linearly stable schemes with greater formal order of accuracy than the DG method.

Keywords High-order methods · Flux reconstruction · Discontinuous Galerkin · Stability · Superconvergence

1 Introduction

Existing second-order numerical methods, used widely within industry, have had a successful history solving a large number of problems of engineering interest. However, there has been increasing interest in solving complex flows that are highly separated or vortex dominated and for these problems existing methods have proved unreliable due to excessive numerical dissipation introduced through the lower order spatial discretization. High-order methods offer the prospect of more accurate simulations of these currently intractable problems, but more widespread utilization of these schemes has been hindered in part by their complexity.

✉ J. Romero
jdromero@stanford.edu

[1] Department of Aeronautics and Astronautics, Stanford University, Stanford, CA 94305, USA

Published online: 29 August 2015

One of the more widely used high-order methods for unstructured grids is the discontinous Galerkin (DG) method [11] and its variants [1,3], which discretize the numerical solution through expansions using piecewise discontinuous polynomial basis functions or high-order Lagrange polynomial basis functions in the case of the nodal DG variant [4,5]. The DG schemes are based on a governing system in integral form, incurring the computational cost of numerical quadrature operations. To reduce this expense, a variety of similar numerical schemes, based on the differential form of the governing equations have emerged. The flux reconstruction (FR) approach [7], introduced by Huynh in 2007, defined a general unifying framework that recovers several of these differential schemes for linear fluxes, including the spectral difference (SD) method [9,10], as well as a particular nodal DG scheme. The flexibility of this method is attained through the choice of a correction polynomial used to reconstruct a globally continuous flux from the piecewise discontinuous flux across the domain. In general, the definition of the correction polynomial is somewhat arbitrary with constraints only imposed on element boundaries. While this adds to the flexibility of the framework, the use of such functions also adds to both the analytical complexity of these schemes and the computational expense, as the application of the correction functions typically requires a number of distinct computational steps in the course of generating a globally continuous flux. If an alternative formulation could be developed that maintains favorable properties of the FR method and some of its flexibility, while being computationally cheaper and easier to implement, such a scheme would be a great step towards the wider utilization of high-order methods.

In this paper, one such simplified formulation is outlined. In this new approach to FR, referred to here as the direct flux reconstruction (DFR) method for convenience, a single Lagrange interpolation operation is used in place of the application of correction polynomials to reconstruct the globally continuous flux used for solution advancement. While reducing both the computational and theoretical complexity, this new scheme can also be shown to recover the same nodal DG scheme as the standard FR method with the proper selection of solution collocation points. Additionally, alternative stable schemes can be generated by modifying the locations of the solution points.

This paper begins with a brief review of the FR method. This is followed by description of the DFR approach and the proof of equivalence to the FR formulation of the nodal DG scheme provided the interior solution collocation points are located at the zeros of a Legendre polynomial of corresponding order. An additional proof of the stability of this formulation is then provided, followed by a description of a new family of linearly stable schemes enabled through alternate solution point selection. The formal order of accuracy and linear stability of these schemes is investigated using von Neumann analysis, and variations with greater formal order of accuracy than the DG scheme are defined. Finally, numerical tests are carried out to verify the accuracy and stability results.

2 Review of Flux Reconstruction in 1D

In order to present the simplified formulation, a review of the existing FR methodology is required. More detailed explainations can be found in [7,13]. Consider the 1D scalar conservation law

$$\frac{\partial u}{\partial t} + \frac{\partial f(u)}{\partial x} = 0 \tag{1}$$

where x is the spatial coordinate, t is time, $u = u(x,t)$ is a conserved scalar quantity and $f = f(u)$ is the flux, defined on a closed interval Ω. Consider partitioning Ω into N non-overlapping elements, each denoted by $\Omega_j = \{x | x_j < x < x_{j+1}\}$ such that

$$\Omega = \bigcup_{j=1}^{N} \Omega_j \tag{2}$$

With the domain partitioned, the exact solution u in Eq. (1) can be approximated by numerical solutions u_j^δ which are defined as polynomials of degree P within each Ω_j and exactly zero outside the element. The piecewise sum of such polynomials results in the global approximation u^δ to the exact solution which is generally discontinuous between elements. Similarly, the exact flux $f(u)$ in Eq. (1) can be approximated by fluxes f_j^δ which are defined as polynomials of degree $P+1$ within each Ω_j and exactly zero outside the element. The piecewise sum of these polynomials results in the global approximation f^δ which is C^0 continuous between elements. It is essential that f^δ maintains C^0 continuity between elements in order for the scheme to remain conservative. The procedure to generate the approximate f^δ meeting this requirement, the core of the FR methodology, is outlined in the remainder of this section.

In general, an isoparametric mapping is introduced to transform each element Ω_j to a standard element $\Omega_{js} = \{r| -1 < r < 1\}$

$$r = \Gamma_j(x) = 2\left(\frac{x - x_j}{x_{j+1} - x_j}\right) - 1 \tag{3}$$

$$x = \Gamma_j(r)^{-1} = \left(\frac{1-r}{2}\right)x_j + \left(\frac{1+r}{2}\right)x_{j+1} \tag{4}$$

Applying this transformation gives rise to a transformed equation within the jth standard element Ω_{js} of the following form

$$\frac{\partial \hat{u}_j^\delta}{\partial t} + \frac{1}{J_j}\frac{\partial \hat{f}_j^\delta}{\partial r} = 0 \tag{5}$$

where

$$\hat{u}_j^\delta = u_j^\delta\left(\Gamma_j^{-1}(r), t\right) \tag{6}$$

and

$$\hat{f}_j^\delta = f_j^\delta\left(\Gamma_j^{-1}(r), t\right) \tag{7}$$

J_j is the determinant of the element Jacobian, $J_j = \frac{1}{2}(x_{j+1} - x_j)$. Henceforth, the hat notation to denote the transformed solution and corresponding transformed flux will be dropped for brevity.

In the first step of the FR method, Eq. (5) is discretized within each element by representing the discontinuous solution u_j^δ and corresponding discontinuous flux $f_j^{\delta D}$ as an expansion using Lagrange polynomials defined on a set of $P+1$ interior solution points

$$u_j^\delta(r) = \sum_{n=1}^{P+1} u_{jn}^\delta l_n \tag{8}$$

$$f_j^{\delta D}(r) = \sum_{n=1}^{P+1} f_{jn}^{\delta D} l_n \tag{9}$$

where u_{jn}^δ and $f_{jn}^{\delta D}$ are the known solution and flux values respectively at interior solution points, r_n, and l_n are the corresponding Lagrange polynomials. At this point, the discontinous solution and flux are both polynomials of degree P.

In the next step, common interface fluxes are introduced by computing the discontinuous solution values on the element interfaces using Eq. (8) and using corresponding interface values in neighboring elements as the left and right states in an appropriate numerical flux formulation for the equation being solved

$$f_j^{\delta L} = F\left(u_{j-1}^{\delta}(1), u_j^{\delta}(-1)\right) \tag{10}$$

$$f_j^{\delta R} = F\left(u_j^{\delta}(1), u_{j+1}^{\delta}(-1)\right) \tag{11}$$

where $F(L, R)$ is the interface flux function and $f_j^{\delta L}$ and $f_j^{\delta R}$ are the common interface flux on the left and right boundaries of the jth element respectively.

The following step is to construct a continuous flux f_j^{δ} such that a piecewise sum results in a globally C^0 continuous flux, f^{δ}, that passes through the common interface flux values at element interfaces. This is accomplished by adding correction functions $g_L(r)$ and $g_R(r)$ to the discontinuous flux $f_j^{\delta D}$. The correction functions are polynomials of degree $P+1$ defined such that $g_L(r)$ takes the value of 1 on the left boundary, 0 on the right boundary, and approximates zero within the element interior, with $g_R(r)$ defined similarly, with the boundaries swapped. The continuous flux is constructed by forming a correction flux

$$f_j^{\delta C}(r) = \Delta f_L g_L(r) + \Delta f_R g_R(r) \tag{12}$$

and adding it to the existing discontinuous flux

$$f_j^{\delta} = f_j^{\delta D}(r) + f_j^{\delta C}(r) \tag{13}$$

with

$$\Delta f_L = f_j^{\delta L} - f_j^{\delta D}(-1) \tag{14}$$

$$\Delta f_R = f_j^{\delta R} - f_j^{\delta D}(1) \tag{15}$$

where $f_j^{\delta C}$ denotes the correction flux which is a polynomial of degree $P+1$ and f_j^{δ} is the resulting continuous flux. This continuous flux is a polynomial of degree $P+1$ which takes the values of the common interface fluxes at the boundaries but does not neccessarily pass through the original values of the discontinuous flux in the element interior.

This continuous flux is then utilized in Eq. (5) with an appropriate time advancement scheme to update the solution within each element:

$$\frac{\partial u_j^{\delta}}{\partial t} = -\frac{1}{J_j}\frac{\partial}{\partial r}\left[f_j^{\delta D}(r) + f_j^{\delta C}(r)\right] \tag{16}$$

3 Simplifications to the FR Method

Although the FR method is conceptually simple, its computational complexity is increased by the introduction of correction polynomials g_L and g_R which serve two purposes:

1. Modify the discontinuous flux function $f_j^{\delta D}$ such that a new continuous flux f_j^{δ} is generated that takes the value of the common interface flux values at the element boundaries while maintaining the original interior flux values in an approximate sense.
2. Increase the order of the discontinuous flux polynomial to degree $P+1$, such that when the spatial derivative in Eq. (5) is evaluated, it is of the same order, P, as the solution term.

In [7], Huynh stresses the importance of the order of the continuous flux polynomial being $P+1$ in order to preserve the original order of the solution polynomial. This makes sense if one considers Eq. (5) in a functional sense, meaning that the spatial derivative of the continuous flux function is applied continuously across the entire element; however, in a numerical implementation of this scheme, the spatial derivative of the continuous flux is used only to modify the solution discretely at the interior solution points, with a subsequent Lagrange interpolation through these updated solution values which defines the updated solution polynomial. Since the number of solution points is kept constant at $P+1$, the solution polynomial is guaranteed to remain of degree P, independent of the order of the continuous flux polynomial. The higher order correction is implicitly projected down to the order of the solution through this collocation projection.

With this mindset, a natural replacement to the procedure to generate a continuous flux, without a definition of correction functions, can be described. Without limiting the resulting continuous flux to be a polynomial of degree $P+1$, consider generating a continuous flux polynomial that takes the value of the common interface fluxes at the element boundaries that also maintains the values of the interior fluxes exactly. This can be accomplished using a single Lagrange interpolation of the form

$$f_j^{\delta}(r) = f_j^{\delta L}\tilde{l}_0(r) + \sum_{n=1}^{P+1} f_{jn}^{\delta D}\tilde{l}_n(r) + f_j^{\delta R}\tilde{l}_{P+2}(r) \tag{17}$$

where $\tilde{l}_n(r)$ are the Lagrange interpolating polynomials defined at $P+3$ collocation points $\{-1, r_1, \ldots, r_{P+1}, 1\}$, which are a combined set of the interior solution points and interface flux points. By this definition, the continuous flux polynomial is of degree $P+2$, as opposed to a polynomial of degree $P+1$ in the standard FR formulation. In this formulation, the correction functions are applied implicitly through the Lagrange interpolation procedure, with the choice of solution point locations coupled to the resulting implicit correction function. The remaining steps of the FR scheme are unchanged. For the remainder of this article, this modified scheme will be referred to as the direct Flux Reconstruction (DFR) method.

One major facet of this new formulation is that the continuous flux is obtained directly from the known discontinuous flux values in the element interior and the computed common interface fluxes in a single computational step. This is in contrast to the standard formulation using correction functions that requires several distinct computational steps to develop the continuous flux: an extrapolation of the discontinuous flux to the element boundaries, computation of the correction function scalings Δf_L and Δf_R, and the subsequent addition of the scaled correction polynomials to the existing discontinuous flux. Additionally, even without the explicit definition of correction polynomials, some of the flexibility of the FR formulation is maintained, through the possibility of modifying the solution point locations within an element.

4 Recovery of the Nodal Discontinuous Galerkin Scheme

4.1 Preliminaries

As described previously, the contribution of the spatial derivative of the continuous flux is only applied discretely at the interior solution point locations within an element. With that being the case, the DFR scheme can be made to recover an existing variant of the FR scheme if the interior solution point locations are selected such that

$$\frac{\partial}{\partial r}\left(f_j^{\delta} - f_{j\,\mathrm{DFR}}^{\delta}\right)\Big|_{r=r_n} = 0 \quad \text{for} \quad n = 1, \ldots, P+1 \tag{18}$$

where f_j^{δ} and $f_{j\,\mathrm{DFR}}^{\delta}$ are the continuous fluxes from the standard FR method and the DFR method respectively.

If Eq. (18) holds, the discrete solution update will be equivalent between the two schemes. It is shown next that if the interior solution points are placed at the zeros of a Legendre polynomial of appropriate order, the DFR formulation recovers the nodal DG variant of the FR scheme.

4.2 Proof of Equivalence

The DFR continuous flux, defined by Eq. (17), can be expressed as a sum of the discontinuous flux $f_j^{\delta D}$ and an effective correction flux $f_{j\,\mathrm{DFR}}^{\delta C}$

$$f_{\mathrm{DFR}}^{\delta} = f_j^{\delta D} + f_{j\,\mathrm{DFR}}^{\delta C} \tag{19}$$

which may be compared to the equivalent formula from the standard FR method

$$f_j^{\delta} = f_j^{\delta D} + f_j^{\delta C} \tag{20}$$

On substitution into Eq. (18), the requirement for equivalency now reduces to

$$\frac{\partial}{\partial r}\left(f_j^{\delta C} - f_{j\,\mathrm{DFR}}^{\delta C}\right)\Big|_{r=r_n} = 0 \quad \text{for} \quad n = 1, \ldots, P+1 \tag{21}$$

Moreover, the DFR correction flux can be expressed in terms of effective left and right correction functions, $g_{L\,\mathrm{DFR}}$ and $g_{R\,\mathrm{DFR}}$ as

$$f_{j\,\mathrm{DFR}}^{\delta C} = \Delta f_L g_{L\,\mathrm{DFR}} + \Delta f_R g_{R\,\mathrm{DFR}} \tag{22}$$

which may be compared to the equivalent formula from the standard FR method, Eq. (12). Subtracting Eqs. (22) and (12), taking a derivative, and substituting into Eq. (21) gives

$$\Delta f_L \frac{d}{dr}(g_L - g_{L\,\mathrm{DFR}})\Big|_{r=r_n} + \Delta f_R \frac{d}{dr}(g_R - g_{R\,\mathrm{DFR}})\Big|_{r=r_n} = 0 \tag{23}$$

Since Δf_L and Δf_R are arbitrary, it is required to prove

$$\frac{d}{dr}(g_L - g_{L\,\mathrm{DFR}})\Big|_{r=r_n} = 0 \tag{24}$$

$$\frac{d}{dr}(g_R - g_{R\,\mathrm{DFR}})\Big|_{r=r_n} = 0 \tag{25}$$

to prove scheme equivalency.

It is known that to recover the nodal DG scheme using the standard FR methodology, one requires correction functions of the form

$$g_L = \frac{(-1)^P}{2}(L_P - L_{P+1}) \tag{26}$$

$$g_R = \frac{1}{2}(L_P + L_{P+1}) \tag{27}$$

which are the right and left Radau polynomials respectively, with L_P representing the Legendre polynomial of degree P [7]. If the interior solution points using the DFR scheme are

located at the zeros of the Legendre polynomial of degree $P+1$, the effective correction functions that result from the Lagrange interpolation in Eq. (17) can be expressed in terms of Legendre polynomials as

$$g_{L\mathrm{DFR}} = \frac{(-1)^P}{2}(r-1)L_{P+1} \tag{28}$$

$$g_{R\mathrm{DFR}} = \frac{1}{2}(r+1)L_{P+1} \tag{29}$$

To satisfy Eq. (25), consider a residual defined as

$$D = \frac{d}{dr}(g_R - g_{R\mathrm{DFR}}) = \frac{1}{2}\left[\frac{d}{dr}L_P - L_{P+1} - r\frac{d}{dr}L_{P+1}\right] \tag{30}$$

Some useful formulae from [6] are listed below

$$(1-r^2)\frac{d}{dr}L_{P+1} = (P+1)\left[L_P - rL_{P+1}\right] \tag{31}$$

$$(1-r^2)\frac{d}{dr}L_P = (P+1)(rL_P - L_{P+1}) \tag{32}$$

Substitution of Eq. (31) into Eq. (30) yields

$$D = \frac{1}{2(1-r^2)}\left[(1-r^2)\left(\frac{d}{dr}L_P - L_{P+1}\right) - (P+1)(rL_P - r^2L_{P+1})\right] \tag{33}$$

Substitution of Eq. (32) into Eq. (33) yields

$$D = -\frac{1}{2}(P+2)L_{P+1} \tag{34}$$

At the zeros of L_{P+1}, which correspond to the locations of the interior solution points r_n, the residual is exactly equal to zero and Eq. (25) is satisfied.

Equation (24) can be satisfied in similar fashion. Consider a residual defined as

$$D = \frac{d}{dr}(g_L - g_{L\mathrm{DFR}}) = \frac{(-1)^P}{2}\left[\frac{d}{dr}L_P - L_{P+1} - r\frac{d}{dr}L_{P+1}\right] \tag{35}$$

Observing that the bracketed term in Eq. (35) is identical to the term in Eq. (30), it can be immediately said that

$$D = \frac{(-1)^{P+1}}{2}(P+2)L_{P+1} \tag{36}$$

At the zeros of L_{P+1}, which correspond to the locations of the interior solution points r_n, the residual is exactly equal to zero and Eq. (24) is also satisfied. This proves the equivalence of the DFR scheme to the FR formulation of the nodal DG scheme provided the solution points are located at the zeros of the Legendre polynomial of order $P+1$. Note that this proof extends to nonlinear fluxes as well since no assumption of linearity has been made.

Figures 1 and 2 plot the standard FR correction functions and the effective DFR correction functions and their derivatives with respect to r for $P=2$ and $P=4$. At the vertical lines, which are the locations of the corresponding Legendre zeros, it can be observed clearly that the slopes of the correction functions are equivalent.

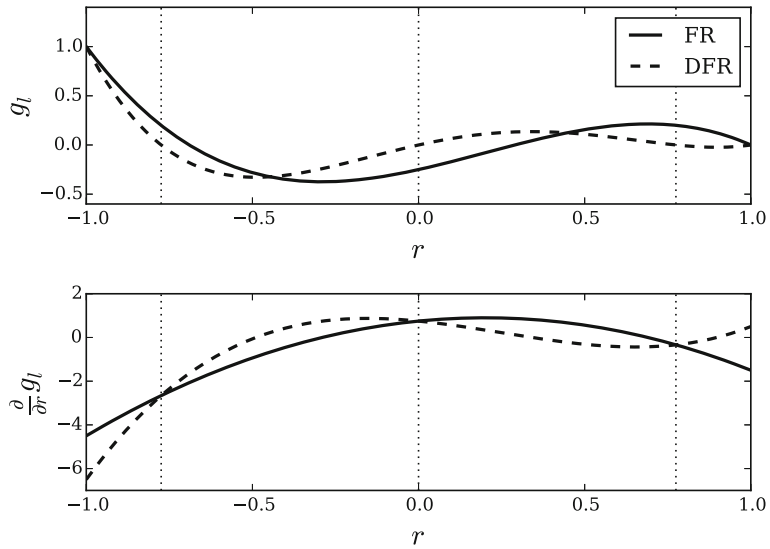

Fig. 1 Left correction function comparison for $P = 2$

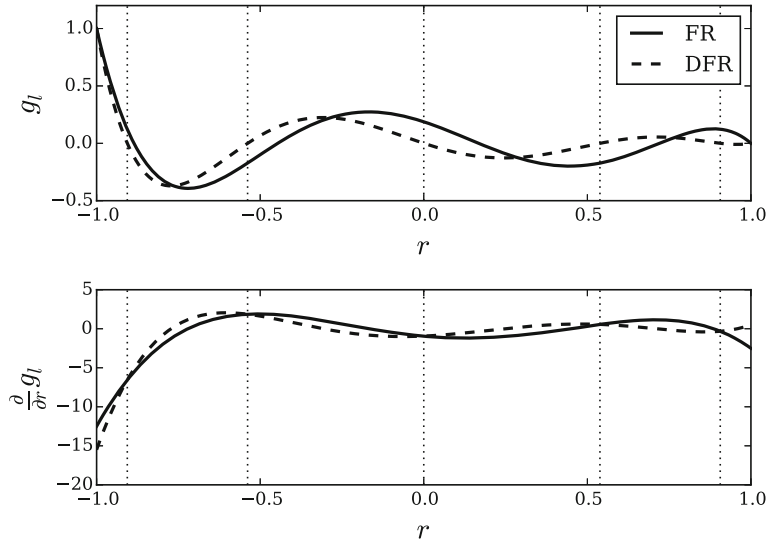

Fig. 2 Left correction function comparison for $P = 4$

5 Proof of Linear Stability

The FR formulation of the nodal DG scheme has been proven to be energy stable for linear fluxes by Vincent et. al. [13]. While the proof in the previous section guarantees that the DFR scheme can recover the nodal DG scheme and, one can assume, maintains its stability properties, a direct stability proof of the nodal DG scheme using this method for linear fluxes is provided for the sake of completeness. This proof borrows much from previous findings by Jameson [8], and Vincent et. al. [13].

5.1 Preliminaries

The update equation for the DFR scheme can be written as follows

$$\frac{du_j^\delta}{dt} = -J_j^{-1}\left[f_j^{\delta L}\frac{d\tilde{l}_0}{dr} + \sum_{n=1}^{P+1} f_{jn}^{\delta D}\frac{d\tilde{l}_n}{dr} + f_j^{\delta R}\frac{d\tilde{l}_{P+2}}{dr}\right] \tag{37}$$

Multiplying Eq. (37) by u_j^δ gives

$$\frac{d}{dt}\left(\frac{(u_j^\delta)^2}{2}\right) = -J_j^{-1}\left[f_j^{\delta L}u_j^\delta\frac{d\tilde{l}_0}{dr} + \sum_{n=1}^{P+1} f_{jn}^{\delta D}u_j^\delta\frac{d\tilde{l}_n}{dr} + f_j^{\delta R}u_j^\delta\frac{d\tilde{l}_{P+2}}{dr}\right] \tag{38}$$

Integrating over the domain results in

$$\frac{d}{dt}\int_{-1}^{1}\frac{(u_j^\delta)^2}{2}dr = -J_j^{-1}\int_{-1}^{1}\left[\underbrace{f_j^{\delta L}u_j^\delta\frac{d\tilde{l}_0}{dr}}_{I} + \underbrace{\sum_{n=1}^{P+1} f_{jn}^{\delta D}u_j^\delta\frac{d\tilde{l}_n}{dr}}_{III} + \underbrace{f_j^{\delta R}u_j^\delta\frac{d\tilde{l}_{P+2}}{dr}}_{II}\right]dr \tag{39}$$

For simplicity, consider the terms of the integrand separately. Integrate term I by parts

$$\begin{aligned} f_j^{\delta L}\int_{-1}^{1} u_j^\delta\frac{d\tilde{l}_0}{dr}dr &= f_j^{\delta L}\int_{-1}^{1}\left[\frac{\partial}{\partial r}(u_j^\delta\tilde{l}_0) - \frac{\partial u_j^\delta}{\partial r}\tilde{l}_0\right]dr \\ &= f_j^{\delta L}\left(\left[u_j^\delta\tilde{l}_0\right]_{-1}^{1} - \int_{-1}^{1}\frac{\partial u_j^\delta}{\partial r}\tilde{l}_0 dr\right) \\ &= -f_j^{\delta L}\left[u_j^\delta(-1) + \int_{-1}^{1}\frac{\partial u_j^\delta}{\partial r}\tilde{l}_0 dr\right] \end{aligned} \tag{40}$$

Note that the first term in Eq. (40) simplified due to $\tilde{l}_0$ being a Lagrange polynomial equal to 1 at $r = -1$ and 0 at all other solution points.

Now, consider the second term in Eq. (40). Since $\frac{\partial u_j^\delta}{\partial r}$ is a polynomial of degree $P-1$ and $\tilde{l}_0$ is a polynomial of degree $P+2$, the integrand is a polynomial of degree $2P+1$. Using Gaussian quadrature, this integral can be exactly computed using $P+1$ quadrature points, leading to a reduced expression for term I

$$\text{I.}\ -f_j^{\delta L}\left[u_j^\delta(-1) + \sum_{q=1}^{P+1} w_q\frac{\partial u_j^\delta}{\partial r}|_{r=r_q}\tilde{l}_0(r_q)\right] \tag{41}$$

where r_q are the quadrature points and w_q are the corresponding weights. A similar expression can be derived for term II

$$\text{II.}\ f_j^{\delta R}\left[u_j^\delta(1) - \sum_{q=1}^{P+1} w_q\frac{\partial u_j^\delta}{\partial r}|_{r=r_q}\tilde{l}_{P+2}(r_q)\right] \tag{42}$$

Integrate term III by parts

$$\int_{-1}^{1} \sum_{n=1}^{P+1} f_{jn}^{\delta D} u_j^{\delta} \frac{d\tilde{l}_n}{dr} dr = \sum_{n=1}^{P+1} f_{jn}^{\delta D} \int_{-1}^{1} u_j^{\delta} \frac{d\tilde{l}_n}{dr} dr$$
$$= \sum_{n=1}^{P+1} f_{jn}^{\delta D} \int_{-1}^{1} \left[\frac{\partial}{\partial r}(u_j^{\delta} \tilde{l}_n) - \frac{\partial u_j^{\delta}}{\partial r} \tilde{l}_n \right] dr$$
$$= -\sum_{n=1}^{P+1} \int_{-1}^{1} f_{jn}^{\delta D} \frac{\partial u_j^{\delta}}{\partial r} \tilde{l}_n dr \tag{43}$$

In this case, the boundary term from the integration vanishes completely, leaving only a single term in Eq. (43). As before, the integrand is a polynomial of degree $2P + 1$ and can be exactly computed using Gaussian quadrature. This leads to a reduced expression of term 3 as

$$\text{III.} \; -\sum_{n=1}^{P+1} \sum_{q=1}^{P+1} f_{jn}^{\delta D} w_q \frac{\partial u_j^{\delta}}{\partial r}|_{r=r_q} \tilde{l}_n(r_q) \tag{44}$$

5.2 Linear Stability Proof for Selection of Solution Points at Zeros of L_{P+1}

If the interior solution points r_n are selected as the Gauss–Legendre quadrature points, which are the zeros of the L_{P+1}, terms I, II, and III can be greatly simplified

$$\text{I.} \; -f_j^{\delta L} \left[u_j^{\delta}(-1) - \sum_{n=1}^{P+1} w_j \frac{\partial u_j^{\delta}}{\partial r}|_{r=r_n} \cancelto{0}{\tilde{l}_0(r_n)} \right] = -f_j^{\delta L} u_j^{\delta}(-1) \tag{45}$$

$$\text{II.} \; f_j^{\delta R} \left[u_j^{\delta}(1) + \sum_{n=1}^{P+1} w_n \frac{\partial u_j^{\delta}}{\partial r}|_{r=r_n} \cancelto{0}{\tilde{l}_{P+2}(r_n)} \right] = f_j^{\delta R} u_j^{\delta}(1) \tag{46}$$

$$\text{III.} \; -\sum_{n=1}^{P+1} \sum_{q=1}^{P+1} f_{jn}^{\delta D} w_q \frac{\partial u_j^{\delta}}{\partial r}|_{r=r_q} \cancelto{1}{\tilde{l}_n(r_q)} = -\sum_{n=1}^{P+1} w_n f_{jn}^{\delta D} \frac{\partial u_j^{\delta}}{\partial r}|_{r=r_n} \tag{47}$$

Now, on substitution back into the integrand of Eq. (39), the resulting expression is

$$\frac{d}{dt} \int_{-1}^{1} \frac{(u_j^{\delta})^2}{2} dr = -J_j^{-1} \left[f_j^{\delta R} u_j^{\delta}(1) - f_j^{\delta L} u_j^{\delta}(-1) - \sum_{n=1}^{P+1} w_n f_{jn}^{\delta D} \frac{\partial u_j^{\delta}}{\partial r}|_{r=r_n} \right] \tag{48}$$

Introduce a linear flux $f_j^{\delta D}(r) = a u_j^{\delta}(r)$ which yields the linear advection equation upon substitution into Eq. (37)

$$\frac{du_j^{\delta}}{dt} = -J_j^{-1} \left[f_j^{\delta L} \frac{d\tilde{l}_0}{dr} + a \sum_{n=1}^{P+1} u_{jn}^{\delta} \frac{d\tilde{l}_n}{dr} + f_j^{\delta R} \frac{d\tilde{l}_{P+2}}{dr} \right] \tag{49}$$

Now Eq. (48) becomes

$$\frac{d}{dt}\int_{-1}^{1}\frac{(u_j^\delta)^2}{2}dr = -J_j^{-1}\left[f_j^{\delta R}u_j^\delta(1) - f_j^{\delta L}u_j^\delta(-1) - a\sum_{n=1}^{P+1} w_n u_{jn}^\delta \frac{\partial u_j^\delta}{\partial r}|_{r=r_n}\right] \tag{50}$$

The last term in (50) can be recast as an integral and evaluated

$$\begin{aligned} a\sum_{n=1}^{P+1} w_n u_{jn}^\delta \frac{\partial u_j^\delta}{\partial r}|_{r=r_n} &= a\int_{-1}^{1} u_j^\delta \frac{\partial u_j^\delta}{\partial r}dr \\ &= a\int_{-1}^{1}\frac{\partial}{\partial r}\left(\frac{(u_j^\delta)^2}{2}\right)dr \\ &= a\left[\frac{u_j^\delta(1)^2 - u_j^\delta(-1)^2}{2}\right] \end{aligned} \tag{51}$$

Now, substitution and transforming the equation back to physical space results in

$$\frac{d}{dt}\int_{x_j}^{x_{j+1}}\frac{u_j^\delta(x)^2}{2}dx = -f_j^{\delta R}u_j^\delta(x_{j+1}) + f_j^{\delta L}u_j^\delta(x_j) + a\left(\frac{u_j^\delta(x_{j+1})^2 - u_j^\delta(x_j)^2}{2}\right) \tag{52}$$

where x_j and x_{j+1} are the locations of the left and right interfaces of the jth element in physical space respectively. Now, introduce upwind biased interface fluxes

$$f_j^{\delta L} = a\left[\frac{u_j^\delta(x_j) + u_{j-1}^\delta(x_j)}{2}\right] - |a|(1-\kappa)\left[\frac{u_j^\delta(x_j) - u_{j-1}^\delta(x_j)}{2}\right] \tag{53}$$

$$f_j^{\delta R} = a\left[\frac{u_j^\delta(x_{j+1}) + u_{j+1}^\delta(x_{j+1})}{2}\right] - |a|(1-\kappa)\left[\frac{u_{j+1}^\delta(x_{j+1}) - u_j^\delta(x_{j+1})}{2}\right] \tag{54}$$

where $0 \le \kappa \le 1$ with $\kappa = 1$ recovering a central scheme, and $\kappa = 0$ recovering a fully upwind scheme. Substituting these definitions into Eq. (52) and summing over j with periodic boundaries gives

$$\frac{d}{dt}\left[\sum_{j=1}^{N}\int_{x_j}^{x_{j+1}}\frac{u_j^\delta(x)^2}{2}dx\right] = -\sum_{j=1}^{N}|a|(1-\kappa)\left[\frac{u_j^\delta(x_j)^2 + u_j^\delta(x_{j+1})^2}{2}\right] \tag{55}$$

Since $0 \le \kappa \le 1$

$$\frac{d}{dt}\left[\sum_{j=1}^{N}\int_{x_j}^{x_{j+1}}\frac{u_j^\delta(x)^2}{2}dx\right] \le 0 \tag{56}$$

This concludes the proof of energy stability for the selection of solution points at the zeros of L_{p+1} for a linear flux.

6 New Family of Schemes

One of the favorable properties of the FR method is the flexibility alloted through the use of alternative correction polynomials. This flexibility has been used to generate schemes that have optimal properties in comparison to the standard DG schemes, such as those with reduced timestep restrictions [14], to schemes with minimal dispersion and dissipation properties [2]. Even with the removal of the explicit definition of the correction polynomials, the DFR scheme retains the ability to generate new schemes through the variation of solution point locations within elements. While many of these variations, as in the FR method, are linearly unstable and of no interest, we present here a subset of these schemes that are linearly stable according to von Neumann analysis.

6.1 Orthogonal Parameterization

In [7], Huynh suggests that the orthogonality of the correction polynomials plays a key role in maintaining the superconvergence properties of the resulting FR schemes. Noting this, consider a parameterization of the solution point locations in the element based on preserving the orthogonality of the effective DFR correction polynomials with respect to the space of all polynomials up to a specified degree q, denoted by $\mathcal{P}_q$.

Note that by construction, the solution point locations within the DFR scheme are collocated with the zeros of the effective implicit correction functions, $g_{L\,\mathrm{DFR}}$ and $g_{R\,\mathrm{DFR}}$. This is due to the fact that the interpolation operation to generate the continuous flux, defined in Eq. (17), preserves the flux values at the solution points, implying that the correction functions are zero at these points within the element. With this being the case, it is possible to define solution points that apply desired implicit correction functions by collocating the solution points with the zeros of the desired correction functions. In the DFR method, the zeros of the left and right correction functions are equivalent and symmetric, so only one correction function needs to be considered. To generate the desired parameterization, it is only required to define a correction function consistent with Eq. (17) that meets orthogonality constraints.

First, define the left correction function to be a polynomial of degree $P+2$ with $P+1$ symmetric interior zeros, and an additional zero at the right element boundary

$$g_{L\,\mathrm{DFR}}(r) = \begin{cases} \alpha(r-1)\prod_{j=1}^{\frac{1}{2}(P+1)}(r^2 - z_j^2) & \text{if } P \text{ odd} \\ \alpha r(r-1)\prod_{j=1}^{\frac{P}{2}}(r^2 - z_j^2) & \text{if } P \text{ even} \end{cases} \tag{57}$$

where the z_j are the $P+1$ interior zeros and α is a constant to scale the correction function such $g_L(-1) = 1$. For the DFR scheme, this constant is not explicitly defined as the interpolation procedure will scale the implicit correction accordingly. In general, the $P+1$ interior zeros, z_j, are the only degrees of freedom in this system, except in the case of P even-ordered, where the central zero is considered to be fixed along with the boundary. Constraining the solution points to be symmetric halves the number of degrees of freedom considered in the system. This leads to an interesting observation that only a single degree of freedom is added for every two orders in P.

To generate correction polynomials that are orthogonal to $\mathcal{P}_q$, the following constraints on the inner product are enforced

$$\int_{-1}^{1} g_{L\,\mathrm{DFR}}(r) L_j dr = 0 \quad \text{for } j = 0, \ldots, q \tag{58}$$

Table 1 Orthogonal parameterizations of DFR solution point locations

P	q	z_1	z_2	z_3
1	0	$\frac{1}{\sqrt{3}}$	—	—
2	0	$\frac{3}{\sqrt{5}}$	—	—
	1			
3	0	$0 < z_1 < \frac{1}{\sqrt{3}}$	$\sqrt{\frac{3-5z_1^2}{5-15z_1^2}}$	—
3	1	$\sqrt{\frac{3}{7} - \frac{2}{7}\sqrt{\frac{6}{5}}}$	$\sqrt{\frac{3}{7} + \frac{2}{7}\sqrt{\frac{6}{5}}}$	—
	2			
4	0	$0 < z_1 < \sqrt{\frac{3}{5}}$	$\sqrt{\frac{3}{7}}\sqrt{\frac{7z_1^2-5}{5z_1^2-3}}$	—
	1			
4	2	$\frac{1}{3}\sqrt{5 - 2\sqrt{\frac{10}{7}}}$	$\frac{1}{3}\sqrt{5 + 2\sqrt{\frac{10}{7}}}$	—
	3			
5	2	$0 < z_1 < \sqrt{\frac{3}{7} - \frac{2}{7}\sqrt{\frac{6}{5}}}$	$f(z1)$	$\sqrt{\frac{1}{7}\left(6 - 7z_1^2 + \frac{1-42z_1^2-49z_1^4}{-6+7z_1^2+63z_1^4+f(z_1)^2}\right)}$
5	3	0.23861919	0.66120939	.093246951
	4			

Solving this system for different combinations of of P and q results in several parameterizations of the solution points that maintain at least the prescribed level of orthogonality. This system was solved symbolically using Mathematica software [15]. These parameterizations can be seen in Table 1. In this table, the function $f(z1)$ for the case $P = 5, q = 2$ is defined to be the third root of the following polynomial $R(x)$, with the roots in ascending order

$$R(x) = \left(63 - 630z_1^2 + 735z_1^4\right)x^4 + \left(-70 + 588z_1^2 - 630z_1^4\right)x^2 + \left(15 - 70z_1^2 + 63z_1^4\right) \tag{59}$$

This polynomial was output from Mathematica in order to represent a zero without an analytic expression. In the table, only the positive zeros are listed in ascending order. The full set of zeros contains the listed zeros, their negative counterparts, and a central zero in the case of P even-ordered.

In general, for a given solution order P, the value of q is limited by the number of degrees of freedom available in the resulting system. However, it is found that for all tested P, the resulting systems contain a number of linearly dependent equations which allow solutions to be obtained for values of $q \leq P - 1$. When $q = P - 1$, the resulting solution is unique and is equal to the zeros L_{P+1}, which corresponds exactly with the DFR formulation of the DG scheme. This is consistent with the findings in [7] in which the correction function in the FR method which recovers the DG scheme is shown to be the only correction function maintaining orthogonality to space $\mathcal{P}_{P-1}$. By reducing q, the system of equations becomes underdetermined, leading to one or more zeros becoming free parameters with defined bounds. These more useful parameterizations are used for the remainder of this paper. Note that these parameterizations include the zeros of L_{P+1} as a possible solution.

6.2 von Neumann Analysis

While the parameterizations above guarantee orthogonality of the correction functions to a specified degree, the resulting schemes may not be linearly stable. To identify a linearly stable family of schemes, von Neumann analysis is carried out over several variations of the solution points, using the developed parameterizations.

The analysis is carried out using the method described in [2]. A brief description of the procedure is provided here, with further detail left to the cited reference. Consider the 1-D conservation equation for advection

$$\frac{\partial u}{\partial t} + \frac{\partial u}{\partial x} = 0 \tag{60}$$

If a fully-upwinded flux is admitted, a numerical update with explicit element coupling is obtained

$$\frac{d}{dt}\mathbf{u}_\mathbf{j}^\delta = -J_n^{-1}\left[\mathbf{C_0}\mathbf{u}_\mathbf{j}^\delta + \mathbf{C_{-1}}\mathbf{u}_\mathbf{j-1}^\delta\right] \tag{61}$$

with

$$\begin{aligned}\mathbf{C_0} &= \mathbf{D} - \mathbf{g}_{\mathbf{L},r}\mathbf{I_L}^T \\ \mathbf{C_{-1}} &= \mathbf{g}_{\mathbf{L},r}\mathbf{I_R}^T\end{aligned} \tag{62}$$

where $\mathbf{I_L}$ and $\mathbf{I_R}$ are vectors containing values of the Lagrange polynomials at the left and right element interfaces respectively, $\mathbf{D}$ is the discrete derivative operator defined such that $D_{ij} = \frac{d}{dx}l_i(r_j)$, and

$$(\mathbf{g}_{\mathbf{L},r})_j = \frac{d}{dr}\left[g_{L\mathrm{DFR}}(r)\right]\Big|_{r=r_j} \tag{63}$$

Note that the bracketed term in Eq. (63) is the effective left DFR correction function generated by the parameterization.

Consider a uniform grid of unit spacing so that $J_j = 1/2$ for $j = 1, ..., N$. Using an initial condition of the form $u(x, 0) = e^{ikx}$ with wave number k, and an associated analytical solution $u(x, t) = e^{ik(x-t)}$, an eigenvalue problem can be formulated

$$\mathbf{M}\mathbf{v} = a^\delta\mathbf{v} \tag{64}$$

where $\mathbf{M}$ is a $(P + 1) \times (P + 1)$ matrix defined as

$$\mathbf{M} = \frac{-2i}{k}(\mathbf{C_0} + e^{-ik}\mathbf{C_{-1}}) \tag{65}$$

and $\mathbf{v}$ is a $(P+1) \times 1$ vector associated with a collocation projection of the analytical solution on to a polynomial space and the eigenvalue a^δ is the numerical wavespeed. Note that this formulation assumes time is integrated exactly. For a given wave number k, solving Eq. (64) results in $P + 1$ eigenmodes with $P + 1$ corresponding complex eigenvalues

$$a_n^\delta(k) = a_{nr}^\delta(k) + ia_{ni}^\delta(k) \quad \text{for} \quad n = 1, 2, ..., P + 1 \tag{66}$$

For a given variation of the DFR scheme to be linearly stable, it is required that the imaginary component of the numerical wavespeed, $a_{ni}^\delta(k)$, is non-positive for all wave numbers $k \in [0, (P + 1)\pi]$ over all $P + 1$ eigenmodes. This metric ensures that the solution amplitude is nonincreasing over all resolvable wavenumbers and over all eigenmodes.

Results from this analysis can be found plotted in Figs. 3 and 4. Figure 3 contains plots of the maximum imaginary wavespeed component over all wave numbers and eigenmodes as a

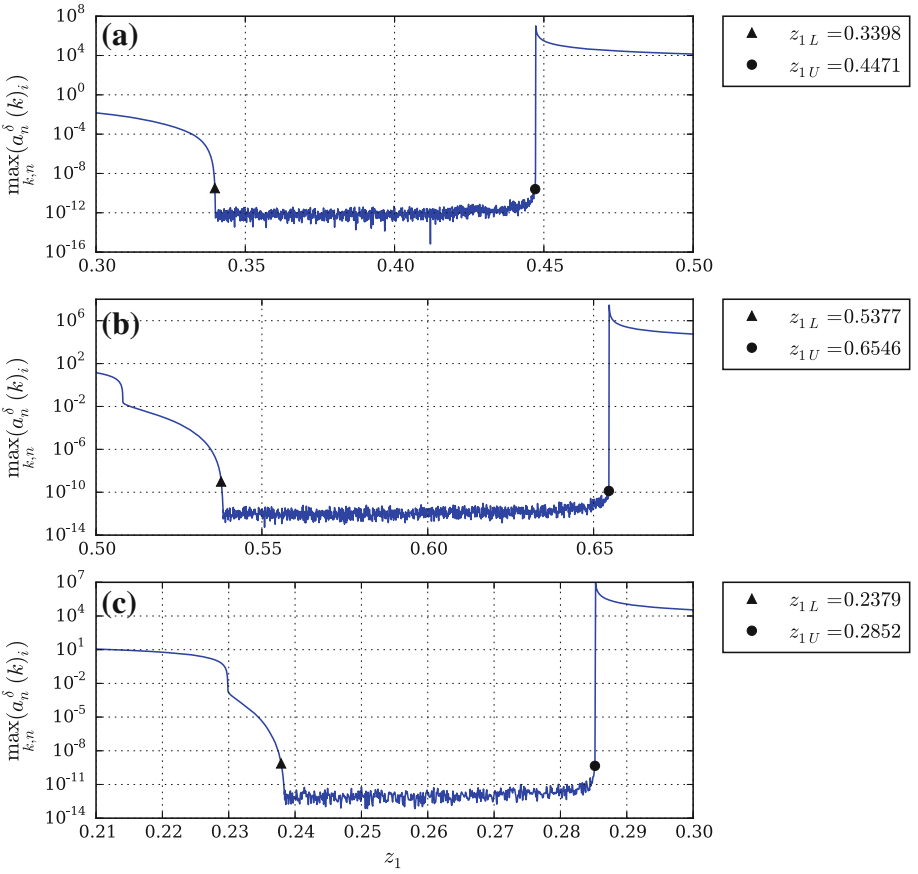

Fig. 3 Plots of $\max_{k,n}(a_{ni}^{\delta}(k))$ versus α and stability bounds ($z_{1L} \leq z_1 \leq z_{1U}$) by polynomial order: **a** $P = 3$, **b** $P = 4$, **c** $P = 5$

function of the free parameter z_1 for various solution polynomial orders. The key observation that can be made from these plots is the existence of a distinct stability region of z_1 for each polynomial order. Approximate upper and lower bounds on z_1 for linear stability derived through this analysis are marked on the plots. Note that due to the numerical nature of this analysis, small positive numbers below a tolerance of 10^{-9} were considered to be stable. This leads to the potential for some of these schemes, if truly unstable, to exhibit only weak instabilities. Figure 4 plots the estimated asymptotic formal order of accuracy as a function of the parameter z_1 for various solution polynomial orders using the method described in [7]. Define an error E

$$E(k) = |a(k) - a_1^{\delta}(k)| \tag{67}$$

where $a(k)$ is the analytical wavespeed of wavenumber k, which is equal to one for all wavenumbers in this case, and $a_1^{\delta}(k)$ is the computed numerical wavespeed of the physical mode, which is generally a complex value. The order of accuracy with respect to the solution can be defined as

$$A = \left(\frac{\ln[E(k)] - \ln[E(k/2)]}{\ln(2)} \right) \tag{68}$$

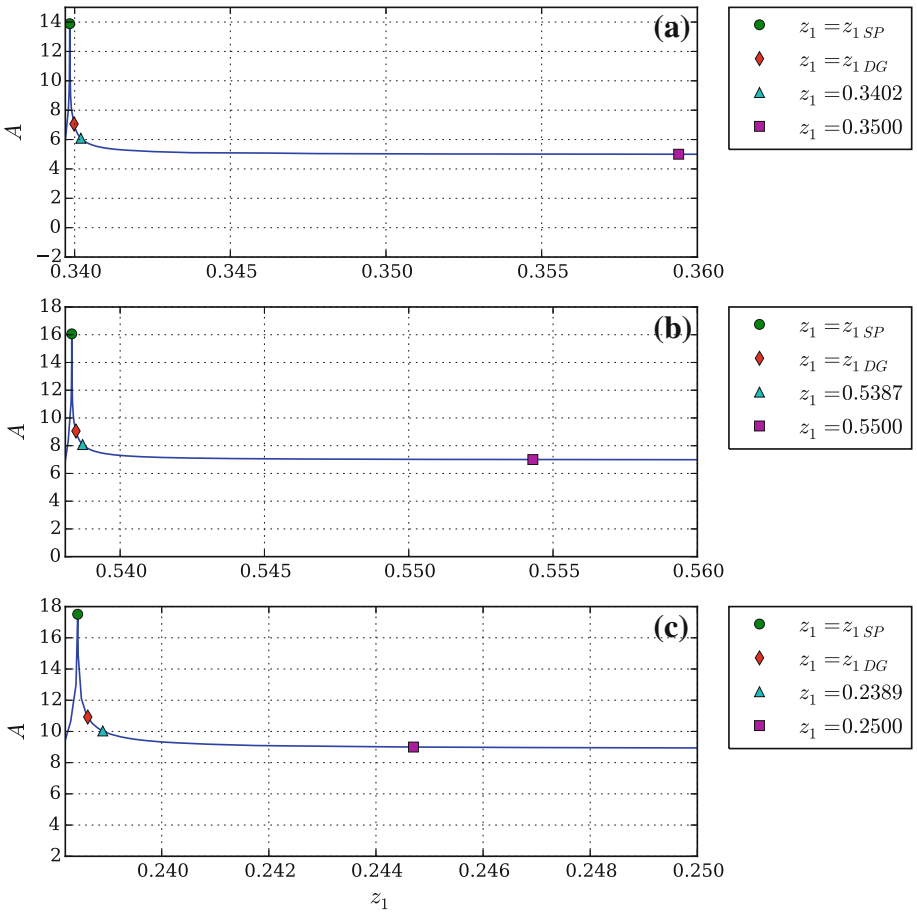

Fig. 4 Plots of formal order of accuracy near left stability boundary by polynomial order: **a** $P = 3$, **b** $P = 4$, **c** $P = 5$

where halving the wavespeed corresponds to a doubling of the grid resolution. Observing the results, all stable variations of the DFR scheme investigated exhibit superconvergence, with $A > P + 1$ across the defined stability regions in z_1. Several representative values of z_1 are marked on the plots, corresponding to various levels of accuracy.

When z_1 is set to $z_{1\,DG}$, defined as the value of z_1 which corresponds to solution points at the zeros of L_{P+1} and recovery of the nodal DG scheme, $A = 2P + 1$ which is consistent with existing results [7,14]. Of greater interest however is the existence of a small region near $z_{1\,DG}$ where the order increases substantially, exhibiting asymptotic convergence rates of nearly $2P + 8$ for all tested orders, falling slightly short only for $P = 5$; however, this shortfall may be attributed to errors associated with double-precision floating point. Further analysis into this phenomenon is beyond the scope of this paper and continued research is being carried out within the context of DFR and standard FR formulations. For this report, the z_1 value at the peak of these curves, denoted $z_{1\,SP}$, is defined and further numerical results using this variant are reported in the subsequent sections. The remaining two values of z_1 marked in the plots correspond to approximate accuracy values of $2P$ and $2P - 1$. The

locations of z_1 for the cases marked on the plot, along with tabulated errors and associated wavenumbers are provided in Table 2. From this table, some additional observations can be made. First, the DFR variant using z_{1SP} only exhibits the extremely high convergence rate at small wavenumbers, which correspond to highly resolved grids, dropping off rapidly as k is increased. It can be noted however that this reduced convergence rate is still greater than or equal to the $2P+1$ order associated with the DG scheme. Additionally, it can be seen that the order of accuracy is correlelated with the actual error magnitudes, with the scheme using z_{1SP} attaining the lowest error, with increases in error using schemes with lower reported orders of accuracy.

7 Numerical Test Cases

7.1 Travelling Wave

To verify the formal order of accuracy results obtained from the von Neumann analysis in the previous section, a grid convergence study is carried out using a modified version of the travelling wave test case in [14]. For this case, the conservation equation is solved using a fully upwinded linear flux, $f(x,t) = u(x,t)$, on the domain $\Omega = [0, 20]$ with an initial condition $u(x, 0) = 0$, which has an exact polynomial representation. A time-dependent boundary condition $u(0, t) = \sin(\pi t/2)$ is prescribed at the left boundary ($x = 0$) with no boundary condition specified at the right boundary ($x = 20$) since a fully upwinded flux is used. For the experiments, the solution is advanced using a fourth order Runge–Kutta timestepping scheme until time $t = 24$, at which a left-to-right travelling wave fills the domain Ω entirely. At this point, a numerical error, $E(x)$, is defined as the difference in the first half wavelength of the wave within $0 \leq x \leq 2$ and a corresponding half wavelength downstream within $16 \leq x \leq 18$

$$E(x) = u^{\delta}(x) - u^{\delta}(x + 16) \quad \text{for} \quad 0 \leq x \leq 2 \tag{69}$$

This definition of error is designed to isolate errors associated with the dispersion and dissipation properties of the spatial advancement from errors introduced through interpolation. As this error definition contains the difference between two polynomial solutions, Gaussian quadrature integration of appropriate strength is used to produce exact error values. As an additional note, the timestep is set small enough so that spatial errors would be the dominant component in the total error.

This test case is carried out using the same parameterizations and z_1 values as in the von Neumann analysis, and the resulting orders of accuracy are computed. The results of this study can be found in Table 3 and Fig. 5. In general, the order of accuracy results from the grid convergence study agree with the results obtained using von Neumann, with similar trends seen in both order of accuracy and error magnitudes. Notably, the high asympototic orders of accuracy for z_{1SP} from the von Neumann analysis are captured in these simulations at the finest grid resolutions, with slightly higher orders achieved for $P = 4$ and $P = 5$. Note that the fine grid resolution in these cases is coarser in order to limit error values to magnitudes within numerical precision.

7.2 Advection of Gaussian Bump

To illustrate the nature of these new schemes and verify their linear stability properties, simulations using the numerical test case from [13] are carried out using a fully upwinded linear flux at the element interfaces. For this case, a Gaussian profile

Table 2 Order of accuracy estimates from von Neumann analysis

z_1	k	$E(k)$	Order
$P=3$			
$z_{1SP}=0.339842589774454$	$\frac{\pi}{2}$	1.4544e−05	
	$\frac{\pi}{4}$	9.6646e−08	7.234
	$\frac{\pi}{8}$	6.3772e−12	13.887
$z_{1DG}=\sqrt{\frac{3}{7}-\frac{2}{7}\sqrt{\frac{6}{5}}}$	$\frac{\pi}{2}$	1.5493e−05	
	$\frac{\pi}{4}$	1.2870e−07	6.912
	$\frac{\pi}{8}$	1.0208e−09	6.978
0.3402	$\frac{\pi}{2}$	1.6997e−05	
	$\frac{\pi}{4}$	1.7944e−07	6.566
	$\frac{\pi}{8}$	2.6373e−09	6.088
0.3500	$\frac{\pi}{2}$	8.667e−05	
	$\frac{\pi}{4}$	2.5330e−06	5.097
	$\frac{\pi}{8}$	7.7614e−08	5.028
$P=4$			
$z_{1SP}=0.538323058771738$	$\frac{2\pi}{3}$	1.4302e−06	
	$\frac{\pi}{3}$	2.4339e−09	9.119
	$\frac{\pi}{6}$	3.557e−14	16.062
$z_{1DG}=\frac{1}{3}\sqrt{5-2\sqrt{\frac{10}{7}}}$	$\frac{2\pi}{3}$	1.5235e−06	
	$\frac{\pi}{3}$	3.2419e−09	8.876
	$\frac{\pi}{6}$	6.4700e−12	8.969
0.5387	$\frac{2\pi}{3}$	1.6708e−06	
	$\frac{\pi}{3}$	4.5177e−09	8.080
	$\frac{\pi}{6}$	1.6694e−11	8.531
0.5500	$\frac{2\pi}{3}$	9.0796e−06	
	$\frac{\pi}{3}$	6.8765e−08	7.015
	$\frac{\pi}{6}$	5.3174e−10	7.045
$P=5$			
$z_{1SP}=0.238431046729096$	$\frac{4\pi}{3}$	2.0203e−05	
	$\frac{2\pi}{3}$	1.0512e−08	10.908
	$\frac{\pi}{3}$	5.6295e−14	17.511
$z_{1DG}=0.238619186083197$	$\frac{4\pi}{3}$	2.1463e−05	
	$\frac{2\pi}{3}$	1.3966e−08	10.898
	$\frac{\pi}{3}$	7.3166e−12	10.586
0.2389	$\frac{4\pi}{3}$	2.3353e−05	
	$\frac{2\pi}{3}$	1.9143e−08	10.253
	$\frac{\pi}{3}$	1.8294e−11	10.031
0.2500	$\frac{4\pi}{3}$	1.0598e−04	
	$\frac{2\pi}{3}$	2.4706e−07	8.745
	$\frac{\pi}{3}$	5.0238e−10	8.942

Table 3 Order of accuracy estimates from grid convergence study

z_1	N	$\|u - u^\delta\|_2$	Order
$P = 3$			
z_{1SP}	20	3.6345e−04	
	40	2.4148e−06	7.2337
	80	1.6378e−10	13.8479
z_{1DG}	20	3.8722e−04	
	40	3.2173e−06	6.9112
	80	2.5520e−08	6.9781
0.3402	20	4.2485e−04	
	40	4.4879e−06	6.5648
	80	6.5990e−08	6.0877
0.3500	20	2.1668e−03	
	40	6.3412e−05	5.0946
	80	1.9432e−06	5.0283
$P = 4$			
z_{1SP}	20	2.6729e−06	
	40	3.4149e−09	9.6124
	60	3.5741e−12	16.9243
z_{1DG}	20	3.0037e−06	
	40	6.1519e−09	8.9315
	80	1.2900e−11	8.8976
0.5387	20	3.5258e−06	
	40	1.0473e−08	8.3951
	80	4.6762e−11	7.8071
0.5500	20	2.9807e−05	
	40	2.2812e−07	7.0297
	80	1.7716e−09	7.0086
$P = 5$			
z_{1SP}	10	2.4833e−05	
	20	8.8437e−09	11.4553
	30	3.3292e−12	19.4462
z_{1DG}	10	2.7626e−05	
	20	1.5607e−08	10.7896
	40	8.7420e−12	10.8020
0.2389	10	3.1873e−05	
	20	2.5824e−08	10.2694
	40	2.9207e−11	9.7882
0.2500	10	2.2453e−04	
	20	4.7825e−07	8.8749
	40	9.5514e−10	8.9678

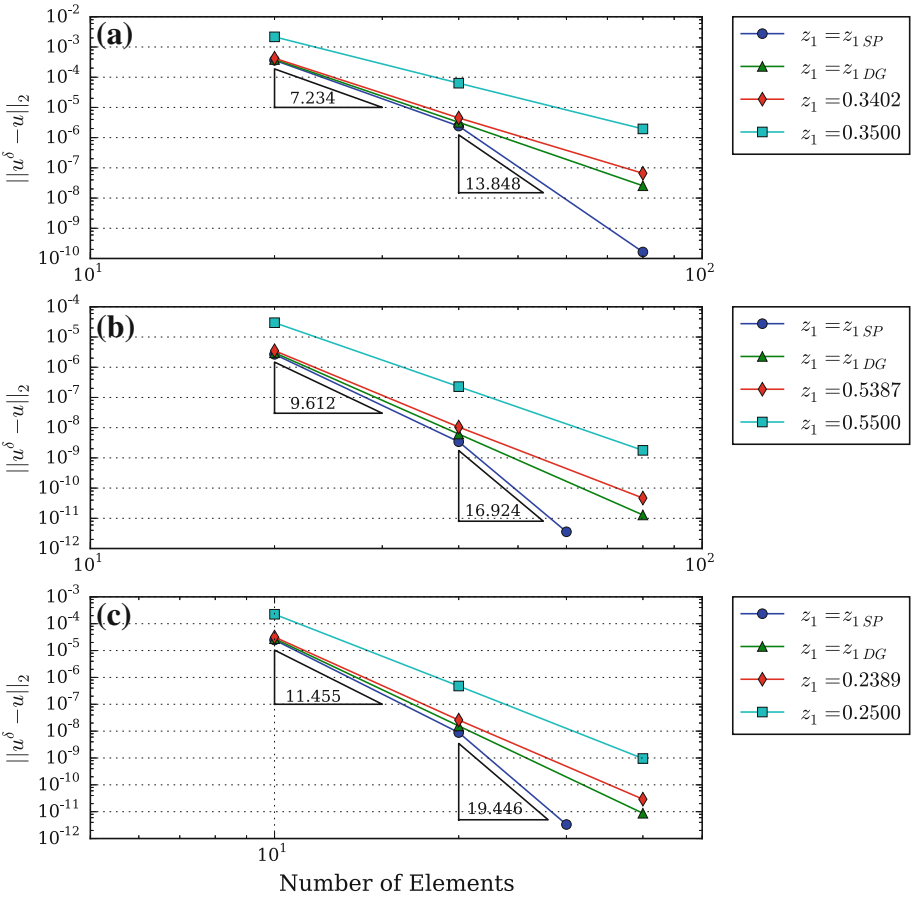

Fig. 5 Error convergence by polynomial order: **a** $P = 3$, **b** $P = 4$, **c** $P = 5$

$$u(x, 0) = e^{-20x^2} \tag{70}$$

is defined on the domain $\Omega = [-1, 1]$ and advected using a linear flux, $f(x, t) = u(x, t)$, with periodic boundary conditions on the ends of Ω. The domain is equally partitioned into N elements, with the number of elements selected to maintain a near equal number of degrees of freedom across all tested polynomial orders. To advance the solution, a standard fourth order Runge–Kutta timestepping scheme is utilized.

The plots in Fig. 6 present the solution after 1000 periods through the domain for the various parameterizations and z_1 values previously defined. Additionally, plots in Fig. 7 present the L_2 energy of the solution, defined as

$$\|u^\delta(t)\|_2^2 = \int_\Omega u^\delta(x, t)^2 dx \tag{71}$$

over the duration of the simulations. In the figures, the period is denoted as T.

Observing the results, schemes using z_1 values closer the left stability boundary better preserve the waveform, with $z_{1\,SP}$ retaining slightly more energy content as compared to the DG variant. However, the amount of dissipation increases rapidly as z_1 tends away from the

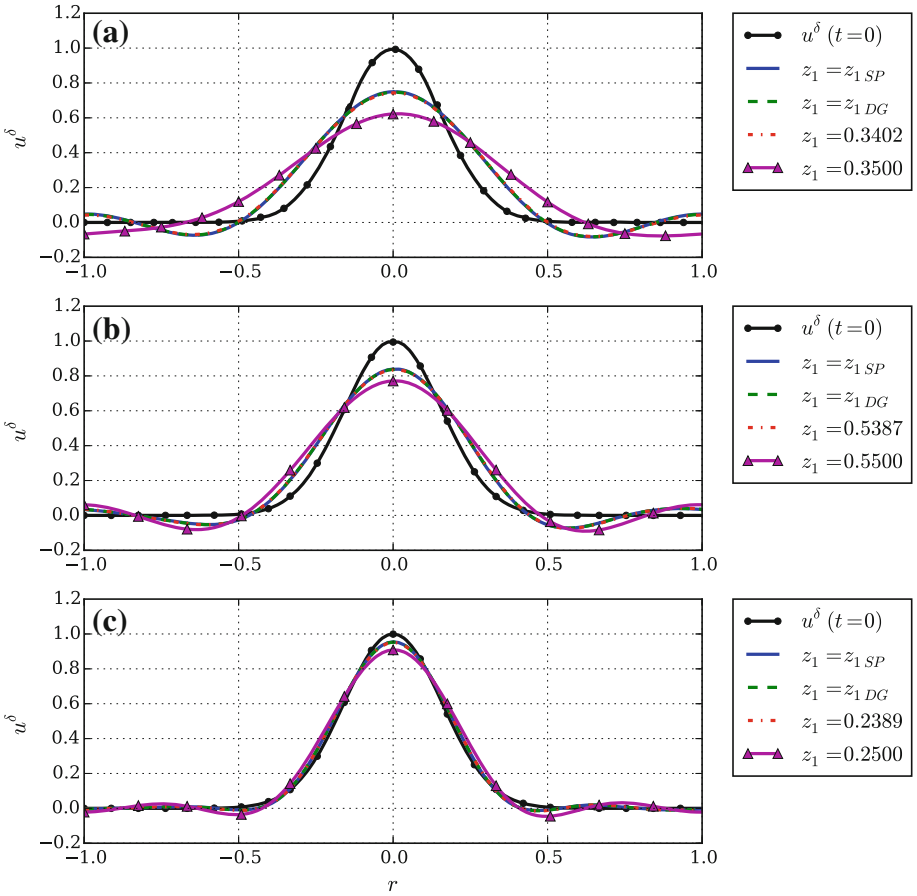

Fig. 6 Comparison of solution by polynomial order, $t/T = 1000$, $T = 2$: **a** $P = 3$, $N = 8$, **b** $P = 4$, $N = 6$, **c** $P = 5$, $N = 5$

stability boundary, with schemes using the largest tested z_1 values showing a much greater loss of energy. Note that for all tested variants, the L_2 energy is strictly decreasing, indicating that these schemes are linearly stable.

7.3 2D Euler Equations: Advection of an Isentropic Vortex

The DFR method can be easily extended to quadrilateral and hexahedral elements using tensor products as described in [7]. The only alteration to the procedure is to swap in the DFR correction operation, described by Eq. (17) in place of the original correction procedure using correction polynomials. To demonstrate this, a numerical test case solving the Euler equations in two dimensions on a quadrilateral mesh is carried out. This test case is also used to verify the recovery of the nodal DG variant of the standard FR method when the solution points are located at the zero of L_{P+1} in both directions of the tensor product for non-linear fluxes.

The Euler equations which describe the flow of a compressible, inviscid fluid can be written in conservation form as

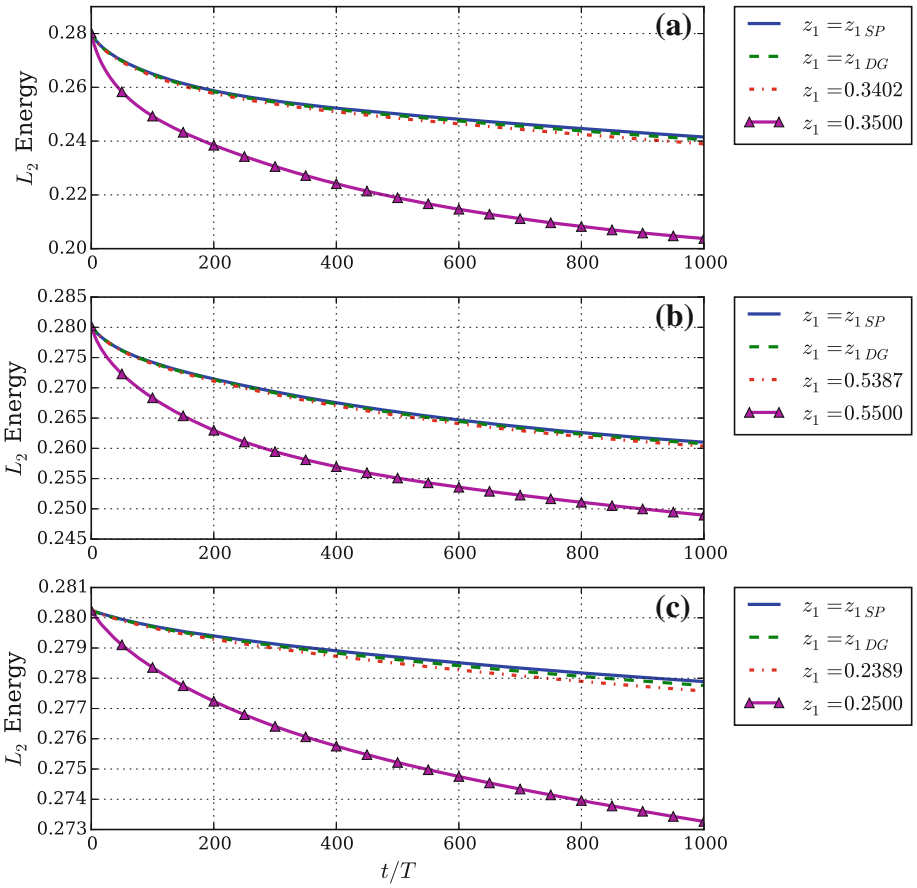

Fig. 7 Comparison of L_2 energy by polynomial order, $T = 2$: **a** $P = 3$, **b** $P = 4$, **c** $P = 5$

$$\frac{\partial \mathbf{U}}{\partial t} + \frac{\partial \mathbf{F}}{\partial x} + \frac{\partial \mathbf{G}}{\partial y} = 0 \tag{72}$$

with

$$\mathbf{U} = \begin{Bmatrix} \rho \\ \rho u \\ \rho v \\ E \end{Bmatrix} \qquad \mathbf{F} = \begin{Bmatrix} \rho u \\ p + \rho u^2 \\ \rho uv \\ u(E+p) \end{Bmatrix} \qquad \mathbf{G} = \begin{Bmatrix} \rho v \\ \rho uv \\ p + \rho v^2 \\ v(E+p) \end{Bmatrix}$$

$$E = \frac{p}{\gamma - 1} + \frac{\rho}{2}(u^2 + v^2)$$

where x and y are the spatial coordinates, t is time, $\rho = \rho(x, y, t)$ is the fluid density, $u = u(x, y, t)$ is the x-velocity, $v = v(x, y, t)$ is the y-velocity, $p = p(x, y, t)$ is the fluid pressure, and the constant $\gamma = 1.4$.

Eq. (72) is solved in a square domain $\Omega = \{x, y | -10 \leq x \leq 10, -10 \leq y \leq 10\}$ with periodic boundaries imposed on all sides. The initial condition is

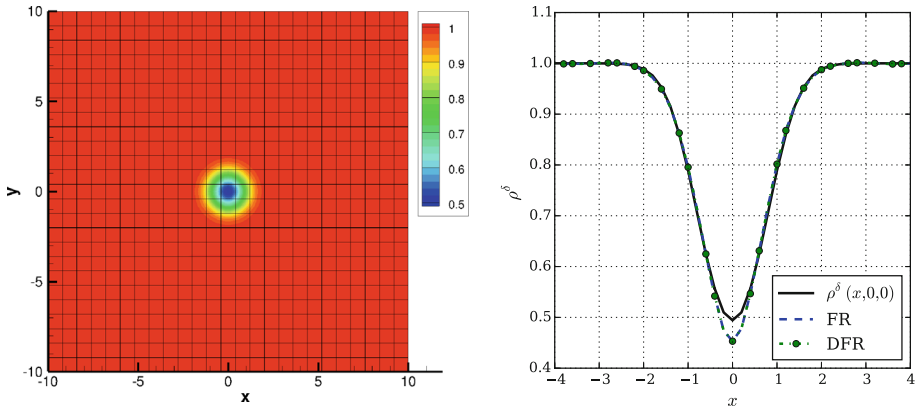

Fig. 8 *Left*: Projection of initial condition of density, $\rho^\delta(x, y, 0)$. *Right*: Numerical density solutions, ρ^δ, along x-axis at $t = 200$

$$\rho(x, y, 0) = \left[1 - \frac{\Gamma^2(\gamma - 1)}{8\gamma\pi^2} e^{2f}\right]^{\frac{1}{\gamma-1}}$$

$$u(x, y, 0) = u_\infty - \frac{\Gamma y}{2\pi} e^f$$

$$v(x, y, 0) = v_\infty + \frac{\Gamma x}{2\pi} e^f$$

$$p(x, y, 0) = \left[1 - \frac{\Gamma^2(\gamma - 1)}{8\gamma\pi^2} e^{2f}\right]^{\frac{\gamma}{\gamma-1}}$$

$$f = \frac{1 - x^2 - y^2}{2}$$

which defines an isentropic vortex of strength Γ and a radius of one in freestream flow with velocities u_∞ and v_∞. For this test case, $\Gamma = 5$, $u_\infty = 1$, and $v_\infty = 1$.

The domain is partitioned into a equispaced grid of 25×25 quadrilateral elements using cubic polynomials within each element to approximate the solution. For this experiment, the common interface fluxes are computed using a fully upwinded Rusanov numerical flux [12] and the solution is advanced in time using a standard fourth order Runge–Kutta timestepping scheme. The initial condition of density, projected onto the discretized domain, can be seen in Fig. 8.

To verify the recovery of the nodal DG variant of the standard FR method, this test case is carried out using both the DFR and standard FR methods with solution points in each tensor product direction located at the zeros of L_{P+1}. For the FR case, the left and right correction polynomials are set to Eqs. (26) and (27) respectively, which recover the nodal DG variant of the standard FR scheme. For each method, the vortex is advected until $t = 200$ at which point the discrete L2 norm of the difference in the numerical density solution between the two schemes at the solution points is computed. A plot comparing the final numerical density solutions along the x-axis, $\rho^\delta(x, 0, 200)$, of both schemes is presented in Fig. 8.

The resulting L2 norm of the difference in numerical density solution of the two schemes at the solution points at the final time, $t = 200$, is computed to be 9.1749×10^{-11}. This value is well within errors associated with numerical precision, indicating that the two schemes are equivalent. This equivalence is further illustrated by Fig. 8, in which the two numerical solution curves are indiscernible. This verifies that the DFR method recovers the nodal DG

variant of the standard FR method for non-linear fluxes, provided the solution points in both tensor product directions are located at the zeros of L_{P+1}.

8 Conclusion

The DFR method appears to be a favorable new variant of the FR approach for solving hyperbolic partial differential equations. This method has been proven to recover the existing FR implementation of the nodal DG scheme using a much simplified correction procedure. Additionally, a family of linearly stable schemes enabled through this method has been identified with variants that exhibit asymptotic convergence at rates greater than $2P + 1$.

A major insight that can be gained from this work is in regard to the true flexibility of the FR method. While previous results have suggested the necessity of correction functions of degree $P + 1$, the DFR method has shown that such a requirement is not necessary and that new stable families of FR schemes can be generated using higher degree correction polynomials. Additionally, preliminary studies suggest that stable variations of the FR method with asymptotic orders of accuracy greater than $2P + 1$, are achievable. Future investigation will be required to determine the nature of this phenomenon as well as the utility of the resulting schemes to real-world applications.

Acknowledgments The first author would like to acknowledge support from the Morgridge Family Stanford Graduate Fellowship. The second author would like to acknowledge support from the Thomas V. Jones Stanford Graduate Fellowship.

References

1. Arnold, D.N., Brezzi, F., Cockburn, B., Marini, L.D.: Unified analysis of discontinuous Galerkin methods for elliptic problems. SIAM J. Numer. Anal. **39**, 1749 (2001)
2. Asthana, K., Jameson, A.: High-order Flux Reconstruction Schemes with Minimal Dispersion and Dissipation. J. Sci. Comput. **62**, 913 (2015)
3. Cockburn, B., Shu, C.: Runge–Kutta discontinuous Galerkin methods for convection-dominated problems. J. Sci. Comput. **16**, 173 (2001)
4. Hesthaven, J.S., Warburton, T.: Nodal high-order methods on unstructured grids. J. Comput. Phys. **181**, 186 (2002)
5. Hesthaven, J.S., Warburton, T.: Nodal Discontinuous Galerkin Methods- Algorithms, Analysis, and Applications. Springer, Berlin (2008)
6. Hildebrand, F.B.: Introduction to Numerical Analysis. Dover, New York (1974)
7. Huynh, H.T.: A Flux Reconstruction Approach to High-Order Schemes Including Discontinuous Galerkin Methods, AIAA Conference Paper, 2007, p 4079 (2007)
8. Jameson, A.: A Proof of the stability of the spectral difference method for all orders of accuracy. J. Sci. Comput. **45**(1–3), 348–358 (2010)
9. Kopriva, D.A., Kolias, J.H.: A conservative staggered-grid Chebyshev multidomain method for compressible flows. J. Comput. Phys. **125**, 244 (1996)
10. Liu, Y., Vinokur, M., Wang, Z.J.: Spectral difference method for unstructured grids I: basic formulation. J. Comput. Phys. **216**, 780 (2006)
11. Reed, W.H., Hill, T.R.: Triangular Mesh Methods for the Neturon Rransport Equation. Technical Report LA-UR-73-479, Los Alamos National Laboratory, Los Alamos, New Mexico, USA (1973)
12. Rusanov, V.V.: Calculation of interaction of non-steady shock waves with obstacles. J. Comput. Math. Phys. **1**, 267 (1961)
13. Vincent, P.E., Castonguay, P., Jameson, A.: A new class of high-order energy stable flux reconstruction schemes. J. Sci. Comput. **47**(1), 5072 (2011)
14. Vincent, P.E., Castonguay, P., Jameson, A.: Insights from von Neumann analysis of high-order flux reconstruction. J. Comput. Phys. **230**, 81348154 (2011)
15. Wolfram Research, Inc., Mathematica, Version 10.1, Champaign, IL (2015)